Journal of Zhejiang University-SCIENCE A 2026 27(2):169-182
www.jzus.zju.edu.cn; www.springer.com/journal/11582
E-mail: jzus_a@zju.edu.cn

Research Article

https://doi.org/10.1631/jzus.A2400192

Check for updates

Mitigating pre-focal heating using a spherical Fibonacci lattice high-intensity focused ultrasound array and a near-field focusing strategy

Xiongfei QU[1], Nan WU[2], Yazhu CHEN[1], Guofeng SHEN[1]✉

[1]School of Biomedical Engineering, Shanghai Jiao Tong University, Shanghai 200030, China
[2]Shanghai Shende Green Medical Era Healthcare Technology Co., Ltd., Shanghai 200233, China

Abstract: Focus steering technique plays a crucial role in various high-intensity focused ultrasound (HIFU) treatment scenarios. However, due to current technological limitations, the focus quality degrades rapidly and prefocal grating lobes arise with increasing focus-shifting distance, which may adversely affect the safety of the treatment. To enlarge the focal steering range of a phased array, a novel method for array element arrangement is proposed in this study, which can increase both the safety and the efficient steering range of the focus. Additionally, a "near-field focusing" strategy for ablation using an HIFU phased array is introduced. Experimental results demonstrate that this strategy not only effectively reduces the average acoustic intensity at the medium's surface but also inhibits temperature elevation in the prefocal region. Thus, this approach could mitigate the risks of skin burn and abdominal edema during clinical HIFU therapy.

Key words: High-intensity focused ultrasound (HIFU); Phased array; Element arrangement; Focus steering

1 Introduction

High-intensity focused ultrasound (HIFU) has gained clinical acceptance as a technique for delivering high-energy ultrasound waves into the human body, enabling deep thermal ablation of pathological tissue (Haar and Coussios, 2007; Zhou, 2011). Compared to traditional open surgery and minimally invasive procedures such as laparoscopic surgery and radiofrequency ablation, HIFU therapy eliminates the need for cutaneous incisions (Kennedy et al., 2003). In other words, HIFU can selectively ablate the diseased tissue within the target region without damaging the surrounding normal tissue along the acoustic propagation path. HIFU has been successfully applied in the treatment of various human pathologies, yielding favorable therapeutic outcomes (Bachu et al., 2021). For instance, extracorporeal HIFU has been utilized to treat tumors and tissue pathologies affecting organs such as the liver (Ji et al., 2020), uterus (Marinova et al., 2021), pancreas (Zhao et al., 2010), bone (Lam et al., 2015), and brain (Agrawal et al., 2021). Additionally, transrectal HIFU has been employed for the treatment of prostate cancer (Ziglioli et al., 2020) and benign prostatic hyperplasia (Garcia-Gutierrez et al., 2022).

Despite demonstrating favorable clinical treatment outcomes, HIFU ablation procedures still exhibit several limitations. Single-element spherical transducers have superior focusing capabilities, but their focal point remains fixed relative to the transducer's position (Haar and Coussios, 2007). Therefore, achieving complete coverage of the target area in the case of solid tumor ablation requires intermittent movement of the HIFU transducer. However, the focal region volume of HIFU systems utilized in clinical tumor therapy is relatively limited, typically around 10 mm long and 2 mm wide in an ellipsoidal shape (Diederich and Hynynen, 1999).

However, in clinical practice, the volume of solid tumors is typically much larger than a single lesion of the HIFU system. Addressing larger tumors necessitates longer treatment time due to the requirement for periodic pauses to allow for mechanical displacement of the transducer (Ter Haar, 2001; Haar and Coussios,

✉ Guofeng SHEN, shenguofeng@sjtu.edu.cn
Xiongfei QU, https://orcid.org/0000-0003-0597-8916
Nan WU, https://orcid.org/0000-0001-7844-1103

Received Apr. 11, 2024; Revision accepted Sept. 27, 2024;
Crosschecked Sept. 2, 2025; Online first Jan. 21, 2026

2007) and adequate cooling to avoid unwanted tissue damage in front of the focal zone (Damianou and Hynynen, 1993). Furthermore, for the treatment of certain diseases such as prostate cancer and essential tremor, the mechanical displacement of the transducer lacks sufficient degrees of freedom to ensure that its geometric focal point can fully cover the treatment target area (Uchida et al., 2012; Chaussy and Thüroff, 2017; Quadri et al., 2018). This makes focus steering indispensable for HIFU treatment of a wide range of diseases.

To achieve optimal focusing performance, a phased HIFU transducer should have a large aperture. Additionally, it is preferable to use array elements with dimensions smaller than half the wavelength and arrange them in a densely packed configuration (Ellens et al., 2011). However, the implementation of such ideal phased-array HIFU arrays would result in a system that is excessively complex, costly, and prone to low reliability. Moreover, achieving its physical implementation is challenging.

Currently, most clinically used phased-array transducers are based on "medium-scale arrays" (16–1024 elements) with element sizes larger than the wavelength. This introduces several limitations to the HIFU system (Gavrilov and Hand, 2000):

1. The appearance of unexpected grating lobes in the acoustic field reduces the focal pressure gain.

2. The presence of secondary pressure maxima on the focal plane results in unintended damage to sensitive structures around the treatment target.

To address these issues, Gavrilov and Hand (2000) ran numerical simulations and discovered that a random arrangement of elements significantly improved the focusing performance of the array. Goss et al. (1996) used a random arrangement of piston elements on the array surface, which effectively suppressed the occurrence of grating lobes in the near field. Subsequent experiments confirmed the superiority of this random arrangement approach. However, random arrangement often results in rather "random" acoustic performance of the array, which means that to obtain an array distribution with superior acoustic performance, a significant amount of time must be spent evaluating a large number of different randomly distributed element arrays and selecting the best one. Rosnitskiy et al. (2018, 2020) proposed a method for designing fully populated random arrays with equal-area polygonal elements. However, their approach is relatively complex, requiring extended computation time, and exhibits a less effective suppression of grating lobes when the number of elements is small (less than 256). Ramaekers et al. (2017a, 2017b) found that avoiding any form of element symmetry can effectively suppress the generation of near-field grating lobes, and proposed a novel phased array transducer design rule for fully populated arrays based on Fermat's spiral, which allows for the rapid generation of element center positions while avoiding symmetry. However, for the smaller *f*-number spherical arrays, the coverage area of the array is not sufficiently uniform.

Besides, during clinical HIFU treatment, the focal points are densely arranged in the tumor region to ensure complete ablation (Haar and Coussios, 2007). This causes multiple heating of the tumor's anterior region due to the overlap of the acoustic beam, potentially causing skin burns and abdominal edema (Mougenot et al., 2011; Kociuba et al., 2023).

The primary objective of this study was to propose a design methodology for spherical phased arrays based on spherical Fibonacci lattice. This method aims to achieve a uniformly distributed array of elements on a spherical array surface while avoiding element symmetry. By improving the uniformity of element distribution on a spherical surface, it is possible to achieve a more consistent area of elements in subsequent fully populated array designs. This, in turn, enhances the consistency of the impedance of the elements, reduces the complexity of impedance matching, and lowers the cost of the HIFU system. Furthermore, when this arrangement method is applied to phased array HIFU transducers with piston elements, the array exhibits improved beam focusing capabilities and the positions of grating lobes become more fixed. As a result, larger ablation zones can be generated using a rapid focus scanning approach (Daum and Hynynen, 1998) with a "near-field focusing" strategy, while reducing the average acoustic intensity on the skin surface and tissue along the beam path during the ablation process. This can improve the efficiency of clinical treatment while ensuring treatment safety.

2 Materials and methods

2.1 Generation of a spherical Fibonacci lattice

The first step of this method involves generating points on the array surface that are distributed as uniformly as possible and should avoid any form of

symmetry. The notion of a uniform distribution here pertains to a geometric problem (Chukkapalli et al., 1999; Hüttig and Stemmer, 2008). For instance, when attempting to quantify the area of a curved surface, such as a sphere, denoted as S_{surf}, if it is possible to sample a set of N points in a "uniform" manner across the surface, then by counting the number of points, denoted as M, falling within a specific range on the surface, the area within that range can be estimated by $s=\frac{M}{N}\times S_{\text{surf}}$ (González, 2010). Obviously, it is not feasible to use the intersections of longitudinal and latitudinal lines on a sphere to calculate the surface area directly, as the lines near the poles are more densely packed (Klíma et al., 1981). Similarly, using methods such as random points on a sphere (Muller, 1959) is also not suitable, as it would require an extremely large number of points to achieve a roughly equal distribution of random points within a unit area.

Currently, there is no elegant analytical solution available for achieving a perfectly uniform distribution of points on a sphere. Therefore, approximate methods are commonly used. Among the existing methods, two notable approaches stand out in terms of achieving optimal uniformity: the minimal energy method (Rakhmanov et al., 1994; Brauchart and Grabner, 2015) and the Fibonacci lattice method (Swinbank and James Purser, 2006; González, 2010). The minimal energy method involves computationally intensive calculations and provides only numerical solutions. In contrast, the Fibonacci lattice method offers a more concise approach for generating points with a nearly uniform distribution on the sphere.

The essence of a spherical Fibonacci lattice lies in mapping the planar Fibonacci lattice points in the $[0,1)\times[0,1)$ region onto the spherical surface by using the Lambert azimuthal equal-area projection. For a Fibonacci lattice in the $[0,1]\times[0,1]$ plane, the Cartesian coordinates of each point are calculated by

$$\begin{cases} \Phi=\dfrac{1+\sqrt{5}}{2}, \\ x=\dfrac{n-1}{\Phi}\%1, \\ y=\dfrac{n-1}{N-1}, \end{cases} \tag{1}$$

where Φ is the golden ratio, n represents the index of the current point, N denotes the total number of points, the %1 (modulo 1) operator denotes keeping just the fractional part of $(n-1)/\Phi$, and x and y represent the coordinates of the current Fibonacci lattice point. When N=2500, the arrangement of points in the planar Fibonacci lattice is as shown in Fig. 1a.

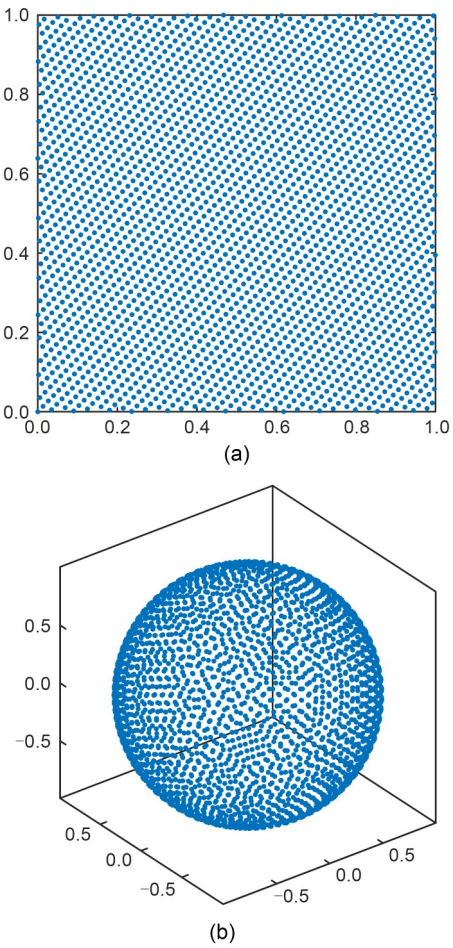

Fig. 1 Distributions of (a) 2500 planar Fibonacci lattice points and (b) spherical Fibonacci lattice with 2500 points

After applying the equal-area transformation (Lambert azimuthal equal-area projection) to Eq. (1), the rearranged equations for the coordinates of spherical Fibonacci lattice points are as follows:

$$\begin{cases} \phi=\dfrac{\sqrt{5}-1}{2}, \\ z_n=\dfrac{2n-1}{N}-1, \\ x_n=\sqrt{1-z_n^2}\cdot\cos(2\pi n\phi), \\ y_n=\sqrt{1-z_n^2}\cdot\sin(2\pi n\phi), \end{cases} \tag{2}$$

where x_n, y_n, and z_n represent the Cartesian coordinates of the current Fibonacci lattice point.

After subjecting the 2500 planar Fibonacci lattice points to the equal-area transformation, their spherical distribution is as shown in Fig. 1b. It is evident that the spherical points obtained through the Fibonacci lattice method have a relatively uniform distribution.

2.2 Phased array models

To evaluate the performance improvement of phased HIFU arrays based on the Fibonacci lattice, two 128-element spherical arrays with identical geometric parameters were generated (with a radius of 160 mm, an *f*-number of about 1.1, and a frequency of 1.1 MHz). One array had a Fibonacci lattice arrangement of 10 mm-diameter piston elements, while the other had a randomly distributed arrangement of 10 mm-diameter piston elements without element symmetry (Figs. 2a and 2b). Note that the acoustic performance of a Fermat spiral array and a Fibonacci lattice array with the same geometric parameters (number of elements, focal radius, and *f*-number) is very similar. Therefore, no comparison of their acoustic performance was made in this study.

2.3 Acoustic modeling and simulation method

To enhance the simulation speed, the effects of nonlinear propagation were not taken into consideration. In this study, simulations for the multilayered media were performed using the hybrid angular spectrum method (HASM) (Vyas and Christensen, 2012). The initial reference plane (100 mm×100 mm, 501 pixels×501 pixels) was oriented perpendicular to the acoustic beam axis and located in paraffin oil, the same medium as the transducer, at an operating frequency of 1.1 MHz. For the phased arrays, this pressure distribution on the initial source plane was obtained using the Rayleigh integral:

$$p(\boldsymbol{r})=\frac{\mathrm{j}\rho ck}{2\pi}\sum_{n=1}^{N}u_n\int_{S_n}\frac{\mathrm{e}^{-(\mathrm{j}k+\alpha)|\boldsymbol{r}-\boldsymbol{r}_n'|}}{|\boldsymbol{r}-\boldsymbol{r}_n'|}\mathrm{d}S_n, \tag{3}$$

where $p(\boldsymbol{r})$ denotes the complex acoustic pressure on the source plane, and $\mathrm{j}=\sqrt{-1}$ is the imaginary unit. The variables ρ and c represent the density and sound speed of the medium, respectively; $k=2\pi/\lambda$ is the wavenumber; S_n and u_n denote the surface area and particle velocity of the nth array element; $\boldsymbol{r}_n'$ represents the center of the $\mathrm{d}S_n$ for the nth element.

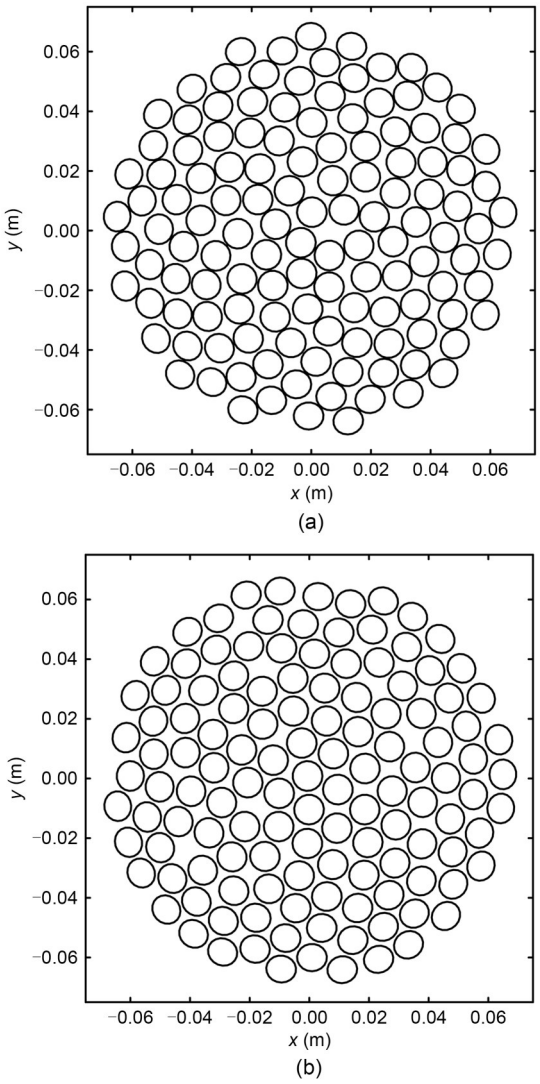

Fig. 2 2D projections of the evaluated array designs based on (a) spherical Fibonacci lattice and (b) random distribution

The steady-state pressure field was propagated plane-wise through the medium stack by incremental steps of Δz=0.2 mm, parallel to the z-axis. First, the spectral propagator was used to obtain the pressure field $p_{n-1}(x, y)$ in the output slice. This pressure field was then calculated as follows:

$$p_n'(x, y)=p_{n-1}(x, y)\mathrm{e}^{\mathrm{j}b_n(x, y)r'}\mathrm{e}^{a_n(x, y)r}, \tag{4}$$

where $b_n(x, y)=2\pi/\lambda_n=2\pi f/c_n(x, y)$ is the propagation constant at various x-y voxel locations, which could be calculated from the specific speed of sound $c_n(x, y)$ and temporal frequency f, $a_n(x, y)$ is the pressure attenuation co-efficient of the individual voxels, and r and r' are constants for a given plane.

The resulting pressure pattern $p'_n(x, y)$ was then Fourier transformed to obtain the angular spectrum $A'_n(\alpha/\lambda, \beta/\lambda; z)$ of traveling plane waves in the spatial-frequency domain before propagation across the plane and these waves travel at different angles that depend on their spatial frequencies f_x and f_y according to direction cosines $\alpha=\lambda f_x$ and $\beta=\lambda f_y$:

$$A'_n\left(\frac{\alpha}{\lambda}, \frac{\beta}{\lambda}; z\right) = \mathcal{F}\{p'_n(x,y)\}. \tag{5}$$

After propagation through the multiple medium layers, the acoustic pressure distribution of each plane could be found from an inverse Fourier transform:

$$p_n(x,y) = \mathcal{F}^{-1}\left\{A_n\left(\frac{\alpha}{\lambda}, \frac{\beta}{\lambda}; z+\Delta z\right)\right\}. \tag{6}$$

Consequently, the propagation of ultrasound waves emitted by the HIFU transducer within a multiple-layer medium could be modeled and the distribution of acoustic pressure in the medium could be calculated.

The acoustic simulation in this study was divided into two parts. In the first part we assessed and compared the focusing quality and beam steering capabilities of two arrays with different element arrangements and performed simulations using degassed water as the medium for sound propagation. In the second part, we simulated the near-field focusing (the focus was electrical steering to the near field) of the spherical Fibonacci lattice array in the human body under clinical treatment conditions. The objective was to determine the optimal near-field focusing distance with no grating lobes with amplitudes above −8 dB occurring. Therefore, a three-layer model was used (Fig. 3), consisting of a 55 mm-thick layer of degassed paraffin oil, a 25 mm-thick water-based coupling pad, and a tissue-mimicking phantom with properties similar to muscle tissue. The acoustic parameters of the four kinds of medium used in the acoustic simulations are listed in Table 1. All numerical simulations were performed within MATLAB R2022a (MathWorks, Inc.).

2.4 Near-field focusing strategy

Typically, when there is effective ultrasound coupling with the skin, the risk of peritoneum burns can be mitigated by reducing the average acoustic intensity at the peritoneum surface. This can be accomplished through two approaches: (1) reducing the output acoustic power of the HIFU transducer; (2) positioning the HIFU transducer closer to the skin, without altering its acoustic power.

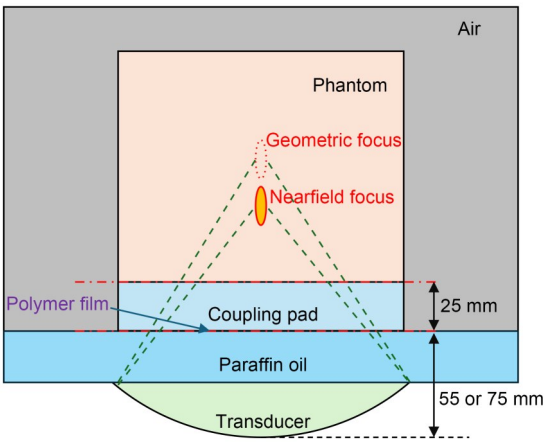

Fig. 3 Illustration of the modeled medium geometry for HIFU sonication

Table 1 Acoustic parameters of different media

Medium	Sound speed (m/s)	Density (kg/m^3)	Attenuation (Np/(m·MHz))
Oil	1420.0	835	0.83
Coupling pad	1482.3	994	0.00
Water	1482.3	994	0.00
Phantom	1508.0	1062	5.79

The first approach is not recommended for clinical HIFU treatments. This is because the sonication time needs to be prolonged to achieve the desired thermal ablation lesion, which would result in significant treatment time extension and potential adverse effects. Consequently, in this case, we considered using the second approach, namely the "near-field focusing" strategy, as illustrated in Fig. 4.

Moving the transducer closer to the skin surface is straightforward. However, it results in the geometric focus being moved to the post-focal region, represented as FocusG in Fig. 4. To address this, electrical beam steering is needed to redirect the focus back to its original position before transducer movement, denoted as FocusN. In this strategy, the circular diameter D_N of the acoustic beam propagating through the skin will be larger than the previous diameter D_O. Consequently, the average acoustic intensity at the skin surface decreases to the previous value of $(D_O/D_N)^2$.

However, if the focus was electrically steered to the pre-focal direction, unexpected grating lobes may

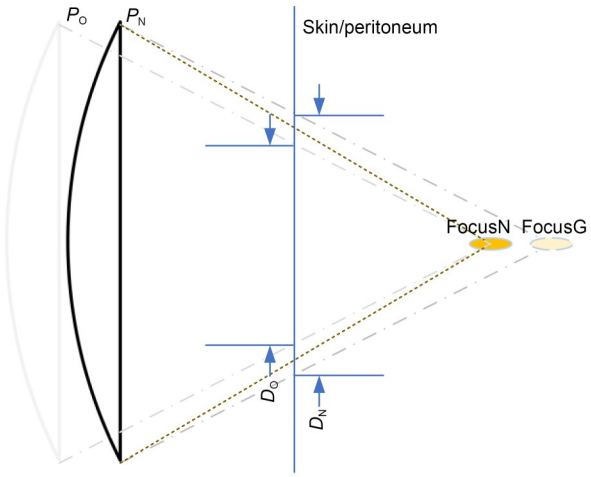

Fig. 4 Schematic diagram of the "near-field focusing" strategy. The geometric focus of the transducer is "FocusG" in the P_N position, "FocusN" in the P_O position, and the "near-field focus" of the transducer in the P_N position

occur in the near-field region, which may result in a decrease in focal pressure. Therefore, it becomes crucial to assess the acceptable range of transducer displacement that can be tolerated without significant negative effects.

2.5 Experimental procedure

The experiment aimed to show that the application of the near-field focusing strategy does not significantly alter the volume of the ablation zone generated by the phase HIFU system using a rapid scanning method. Additionally, we aimed to demonstrate that near-field focusing can reduce thermal damage in the front-field region of the ablation zone, thereby enhancing the safety of HIFU therapy.

A tissue-mimicking phantom was used to simulate human tissue undergoing clinical HIFU treatment. The phantom was composed mainly of degassed water, agar, skimmed milk powder, and a small amount of silica dioxide, with the acoustic parameters detailed in Table 1. To ensure effective ultrasound coupling throughout the entire treatment process and to emulate the tissue depth encountered in clinical applications, a 25 mm-thick water-based coupling pad was placed between the phantom and the paraffin oil tank housing the phased HIFU array. This setup guaranteed optimal ultrasound coupling during the experimental procedure.

A spherical HIFU array with 128 elements was used in the HIFU ablation experiment (with a radius of 160 mm, an *f*-number of about 1.1, and a frequency of 1.1 MHz), which was installed in the ACESO UIA MRgFUS system (Shanghai Shende Medical Technology Co., Ltd., China). The HIFU transducer was adjusted precisely to ensure a distance of about 55 mm between the upper surface of the transducer bottom and the top surface of the paraffin oil tank. A schematic of the experiment is shown in Fig. 3.

The experiments were performed using the Discovery MR750W 3.0T magnetic resonance imaging (MRI) system (GE HealthCare Technologies, Inc., Chicago, USA) for temperature monitoring.

3 Adaptive design model

3.1 Numerical simulation

To compare the uniformity of the distribution of elements of the spherical Fermat's spiral (Ramaekers et al., 2017b) and spherical Fibonacci lattice, both methods were used to generate a piston element arrangement with the same array geometric parameters (a radius of 160 mm, an *f*-number of about 0.51, and N=512).

As shown in Fig. 5, for Fermat's spiral arrangement, the piston elements at the bottom of the spherical cap are sparser, while those on the upper side are more densely packed. This indicates that when designing fully populated arrays with a small *f*-number based on Fermat's spiral, there will be greater inconsistency in the array element size, which in turn increases the difficulty of matching the impedance. While for the spherical Fibonacci lattice, the distribution of elements on the array surface is more uniform, regardless of their location.

To further assess the uniformity of the element area of a fully populated array design using the spherical Fibonacci lattice method, Voronoi tessellation was applied to the 512 spherical Fermat's spiral points and Fibonacci lattice points.

Fig. 6 shows that, compared with the Fermat's spiral array, the element areas of the Fibonacci Lattice array have a high level of uniformity, with all 512 elements area exhibiting deviations within about 6% of the mean value. This clearly highlights the benefits of using this method for generating the element center points in the design and realizing a fully populated array.

For different HIFU array arrangements, there are variations in the quality of focal focusing and the distribution of near-field grating lobes when the focus

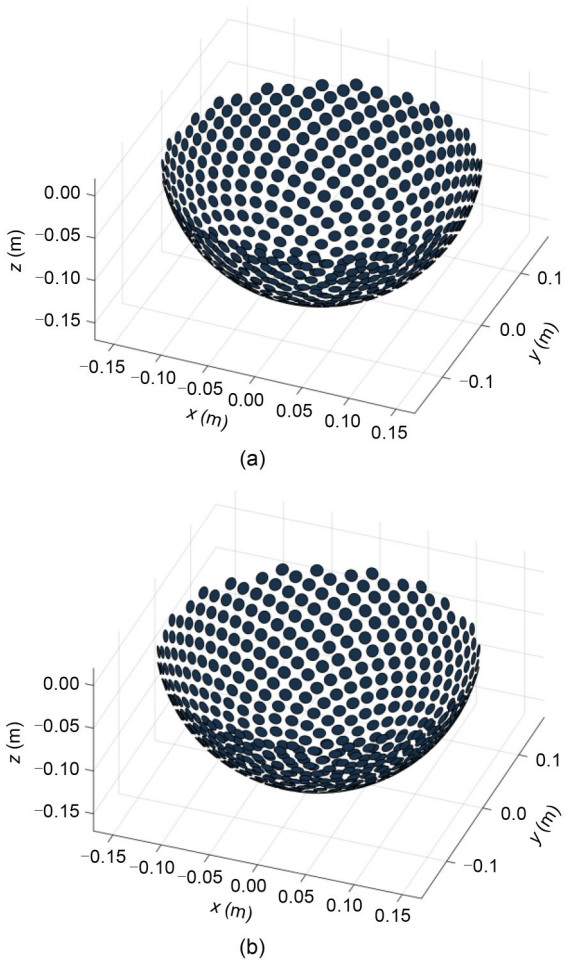

Fig. 5 Distribution of the 512 elements based on (a) Fermat's spiral and (b) Fibonacci lattice

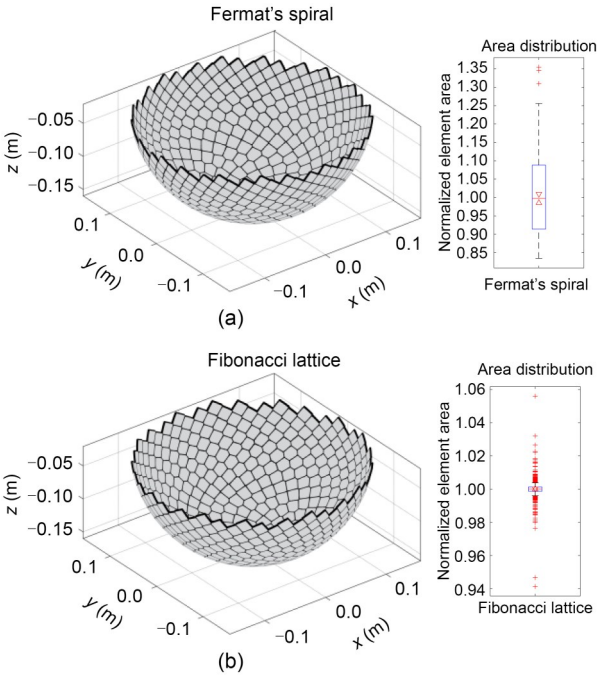

Fig. 6 Illustration of the 512 elements of a fully populated array based on (a) Fermat's spiral and (b) Fibonacci lattice, showing the dispersion of the area for all elements. The polygons represent the 512 array elements obtained by using Voronoi tessellation. References to color refer to the online version of this figure

was electronic steered. To illustrate the differences in performance between the two 128-element arrays, the acoustic field was simulated with the focus unsteered and steered 10 mm laterally (Fig. 7). The pressure field was normalized to the surface pressure of the array surface. The focal pressure gain, as well as the ratio of maximum grating lobe pressure to the main lobe pressure, are annotated in the figure.

Figs. 7a, 7b, 7e, and 7f show that when the focus is not electronically steered, both arrays can achieve a high-quality focal point. The focal pressure gain of the geometric focus for the randomly arranged array is equal to that of the Fibonacci lattice array. This can be attributed to the equal diameters of the elements of the two arrays, which ensures that the two array models have the same total element surface area. When the focus is electronically steered off-axis by 10 mm (Figs. 7c, 7d, 7g, and 7h), both arrays exhibit a noticeable decrease in focal pressure gain. Specifically, the focal pressure gains for the randomly arranged array decrease by 29%, which is more pronounced than the 24% decrease observed for the Fibonacci lattice array.

Moreover, when the focus undergoes off-axis electronic steering, the grating lobe amplitude of the randomly arranged array is significantly higher than that of the Fibonacci lattice array. This implies that, compared to the previously commonly used random arrangement method for designing sparsely distributed arrays, using the Fibonacci lattice method for designing a spherical array can significantly improve the non-axial beam steering performance.

Clearly, this is beneficial for the generation of large ablation zones using the rapid electronic steering of the focus, such as volumetric ablation (Köhler et al., 2009; Kim et al., 2012), because the lower grating lobe amplitudes during non-axial electronic steering can significantly suppress grating lobes in the acoustic field. This, in turn, reduces energy deposition in the surrounding area and along the beam path during the ablation process, thereby improving the safety of the treatment.

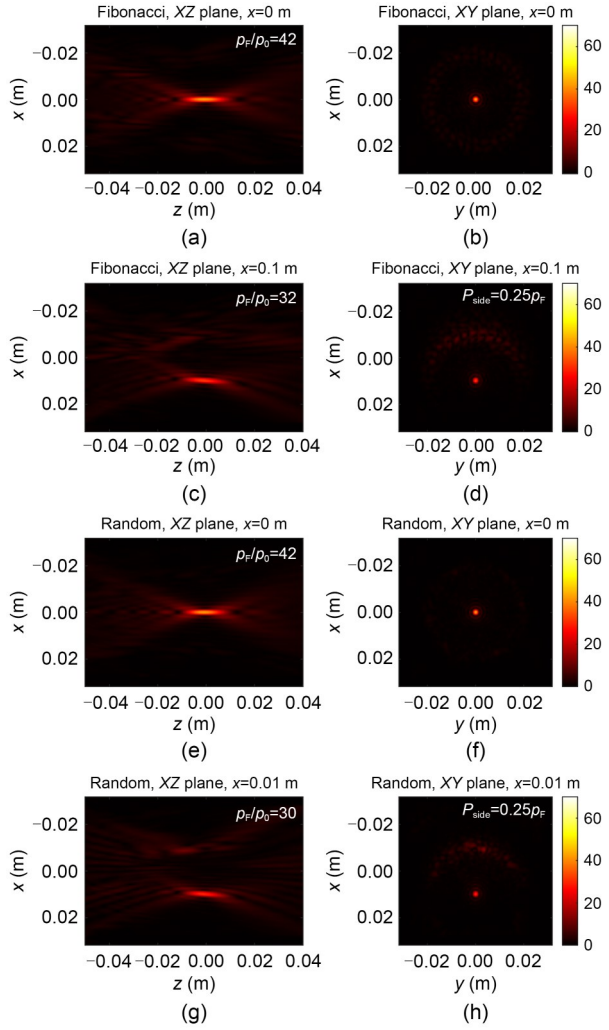

Fig. 7 2D distribution of normalized acoustic pressure p/p_0 for (a)–(d) Fibonacci lattice array and (e)–(h) randomly distributed array. p_0 is the surface pressure of the array, p_F is the maximal focal pressure, and p_{side} is the maximal pressure of the sidelobes

To further evaluate the quality of the shifted focus, the distribution of the acoustic pressure with different shifting distances from −25 to 25 mm axially was calculated, taking into account the focal length and the peak focal pressure (Fig. 8).

Fig. 8 shows that, with increasing distance of focus shifting, the length of the −6 dB focal region gradually elongates, while the peak focal pressure shows an initial rise followed by a decline. At an identical focal steering position, the Fibonacci lattice design has a slightly longer focal region than the random arrangement. Furthermore, compared to the random arrangement, the Fibonacci lattice design shows a slightly higher peak focal pressure within the axial focus

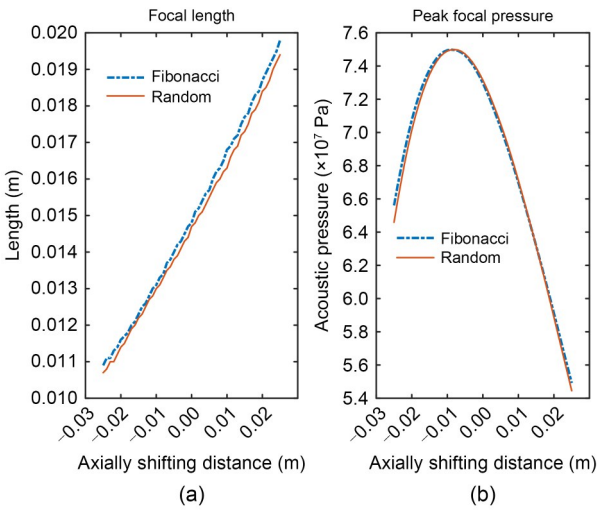

Fig. 8 (a) Length of the focal region (−6 dB) and (b) peak focal pressure for different axial shifting distances

steering range of −25 to −8 mm, as well as from 4 to 25 mm. This indicates a high level of stability in the maximum focal temperature rise when using the HIFU system for ablation within this specific range of focal steering, despite the inherent differences in the ablation volume resulting from changes in the focal length.

To reveal the differences in performance in axial and off-axial focal steering between the two arrays, simulations were conducted of an acoustic field with the focus electronically steered over a significant range in the *XZ* plane. An analysis was performed to ascertain the safe steering range (grating lobe intensity less than −8 dB of the focal intensity) and efficient steering range (peak focal intensity greater than 60% of its maximum achievable value). In other words, within the focus "safe steering range", there will be no significant unintended overheating in the acoustic field; while within the focus "efficient steering range", the energy of the focus will not decrease too significantly.

Fig. 9 shows that for the Fibonacci lattice array, the axial safe steering range of the focus can reach −45 to 45 mm, while the efficient steering range can reach −41 to 34 mm. In comparison, the safe steering range of the randomly arranged array is smaller, only −41 to 40 mm, and the efficient steering range is slightly smaller, from −39 to 30 mm. When it comes to off-axis focal shifting, specifically in the *X*-axis direction, the performance of the Fibonacci lattice array is slightly superior to that of the randomly arranged array, with an 8.0% larger safe steering range and an 8.5% larger efficient steering range. Whether for axial or

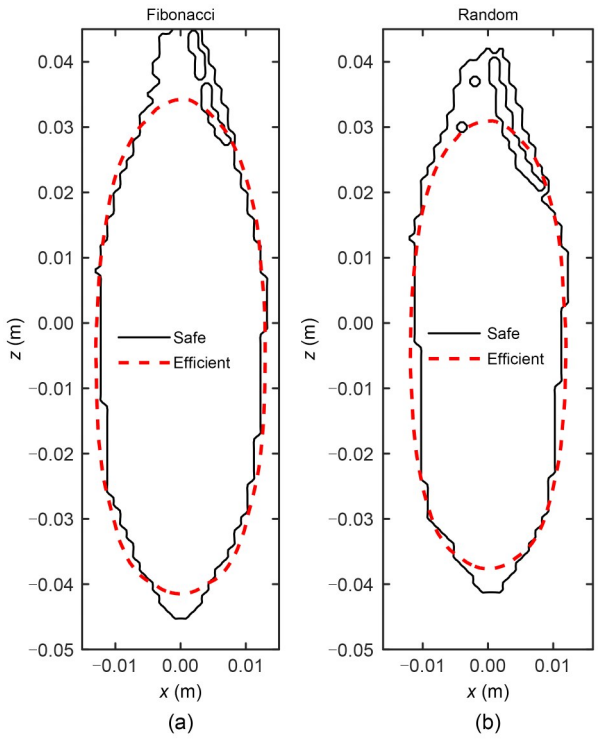

Fig. 9 Contours of the safe and efficient steering ranges for the array based on (a) Fibonacci lattice and (b) Fermat's spiral in the *XZ* plane. The solid line represents the safe range (grating lobe intensity less than −8 dB of the peak focal intensity), and the dashed line represents the efficient range (peak focal intensity greater than 60% of its maximum possible value)

non-axial steering of the focus, the performance of the Fibonacci lattice array surpasses that of the randomly arranged array we previously used.

Due to the superior steering performance of the Fibonacci lattice array, which has a lower peak grating lobe pressure and a milder decrease in maximum focal pressure during axial focal steering, we explored the use of a "near-field focusing" strategy to enhance safety during clinical treatments without a significant reduction in the ablation volume of the ablation zone. In this context, 'safety' refers to a low skin surface temperature rise when the ultrasonic beam propagates from the water coupling pad into the human body, as well as a low temperature rise in the anterior field region of the treatment target, such as the peritoneum or rectus abdominis muscle.

We simplified this intricate process into a concise acoustic model consisting of a three-layered medium (Fig. 3). The model comprised three distinct layers: a 55 mm-deep layer of degassed paraffin oil, a 25 mm-thick water-based coupling pad commonly used in clinical applications, and a sufficiently large-sized phantom. The acoustic parameters characterizing each layer are shown in Table 1.

A simulation was conducted on the acoustic pressure distribution within the specified three-layer medium, considering a focal steering range from −40 to 0 mm axially. Fig. 10 illustrates the axial distribution of acoustic pressure.

When the focus is axially steered to a distance of −20 mm, the axial grating lobes in front of and behind the focus do not show significant enhancement. Moreover, according to the results depicted in Fig. 8b, at this focal steering distance, the focal pressure remains relatively unchanged with no significant decrease.

3.2 Phantom sonication results

We performed six sonications on the tissue-mimicking phantom using the rapid focus scanning mode alone and in combination with the near-field focusing strategy.

Before performing sonication on the phantom, the transducer was meticulously positioned at 55 mm below the 25 mm-thick water-based coupling pad. Subsequently, the focal point was axially steered to a distance of −20 mm. This configuration resulted in an ultrasound propagation depth (the distance from the interface to the focal point) of 60 mm within the phantom. While for sonication without using the near-field focusing strategy, the transducer was positioned at −75 mm below the coupling pad, and the focus was fixed at the geometric center of the spherical transducer.

Each sonication session lasted for 21 s with a fixed acoustic power of 280 W, followed by a natural cooling period of 20 s. The entire process of sonication and cooling was monitored using the magnetic resonance (MR) system. Real-time temperature measurement and calculation of the 240 CEM (cumulative equivalent minutes) region were carried out using the HIFU system software developed by the Shanghai Shende Medical Technology Co., Ltd., China.

Fig. 11 shows that the temperature rises in the vicinity of the sonication area within the phantom appeared to be relatively uniform. The volumes of the ablation zones obtained using both strategies were comparable, with an average of (1842±233) and (1735±147) mm^3, respectively, indicating a moderate level of consistency across multiple sonications.

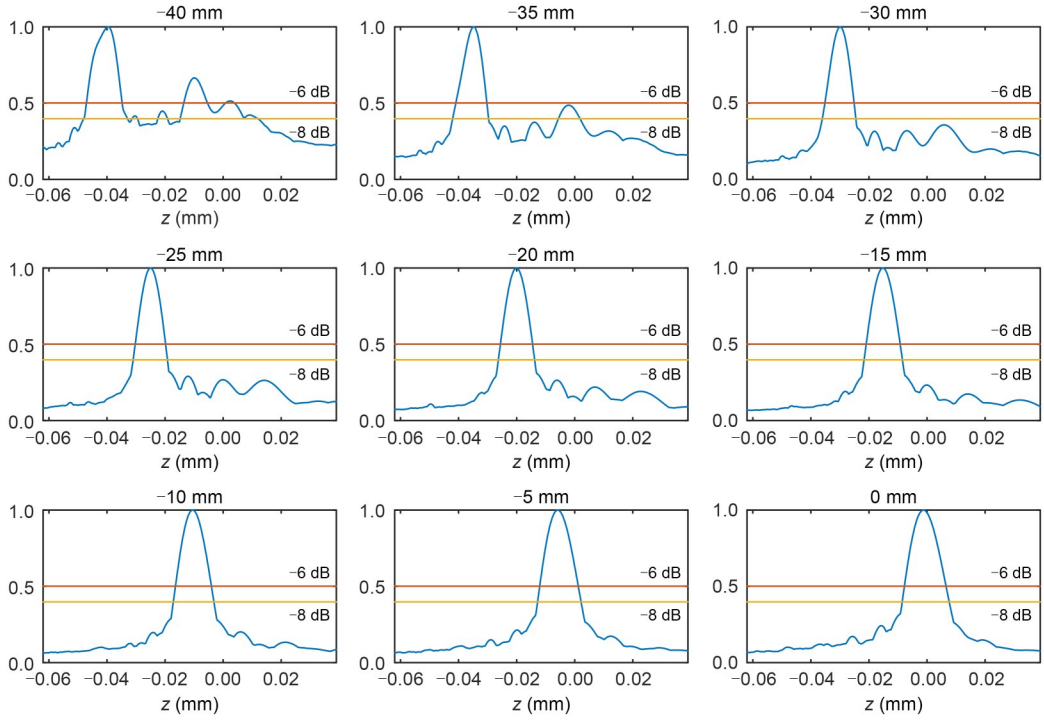

Fig. 10 Axial distribution of sound pressure in the three-layer model for different focal shifting distances

Additionally, at the black arrow positions in Figs. 11a and 11b, which are located about 25 mm before the center of the focal region, there is a significant difference in the peak temperature rise when using two strategies. After implementing the near-field focusing strategy, the peak temperature at that position during the 21-s HIFU sonication reduced from (44.7±1.2) to (41.4±0.9) ℃. Clearly, the peak temperature rise in the pre-focal region along the propagation path of the focused ultrasonic beam will be significantly reduced by combining the near-field focusing strategy.

4 Discussion

Due to constraints imposed by specific application scenarios, many phased HIFU systems are unable to integrate mechanical positioning devices with sufficient degrees of freedom of movement for their transducers, thereby preventing the complete coverage of the required target area by the geometric focus of the transducer. Therefore, it is necessary to integrate the phased array focusing technique into these HIFU devices to ensure their therapeutic efficacy.

However, with the increasing axial or off-axis focal shifting distance, a series of sidelobes will emerge in the pre-focal region, resulting in degradation of the focusing performance of the HIFU. Consequently, although the focus can be steered using beam steering without the need for mechanical movement of the transducer, the presence of these grating lobes diminishes the focusing quality and restricts the focal steering ability.

In this study, we proposed a design method for arranging piston elements in HIFU arrays using a spherical Fibonacci lattice. The array arrangement using the spherical Fibonacci lattice offers a uniform distribution of piston elements on a spherical array surface. To compare the uniformity of the element arrangement generated using Fermat's spiral and the Fibonacci lattice, two transcranial HIFU arrays were created using these two methods. The elements arranged by Fermat's spiral showed significant variation in uniformity at the bottom and upper edges. On the other hand, the array using the Fibonacci lattice showed superior uniformity in element distribution. Applying Voronoi tessellation to the centroid points of the array elements of the transcranial array showed that the fully populated transcranial array generated using the Fibonacci lattice has excellent element area uniformity (with a maximum deviation of about ±8%). This implies that the use of this method is highly promising for

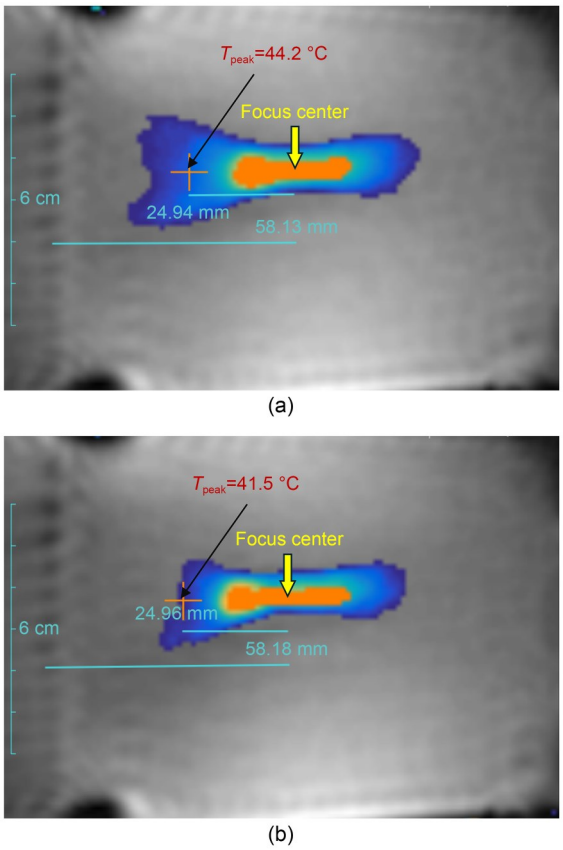

Fig. 11 Results of HIFU sonication using MR thermometry: (a) using the rapid focus scanning mode only; (b) using the rapid focus scanning mode with the near-field focusing strategy. The orange area represents the 240 CEM region, and T_{peak} denotes the maximum temperature of the 25 mm prefocal region during the 21-s HIFU sonication. References to color refer to the online version of this figure

designing fully populated transcranial phased array HIFU transducers in the future.

To reveal the improvement in focusing quality and focal steering capabilities of the phased array designed using the Fibonacci lattice, we conducted an analysis of the main lobe and grating lobes for both HIFU arrays under different focal steering directions and distances. Besides, the Fibonacci lattice array has a lower focal pressure gain than the randomly arranged array. This is because the piston element of the randomly arranged array has a larger diameter, resulting in a higher array filling factor. Furthermore, the randomly arranged array has a higher amplitude of sidelobe pressure during off-axis steering, which may be attributed to the greater element symmetry of the random and dense arrangement compared to the spherical Fibonacci lattice, especially when the element number is small (less than 256) (Rosnitskiy et al., 2020). The Fibonacci lattice array also showed a slightly larger focal size when focus was shifted off-axial. This could be attributed to the sparser distribution of elements at the periphery of the Fibonacci lattice array, which increases the effective *f*-number of the array to some extent, resulting in a slight elongation of the focal zone.

In general, the Fibonacci lattice array showed a larger safe steering range and efficient steering range than the randomly arranged array, regardless of whether axial or off-axis focal steering was performed. The expanded focal steering range of this design remains within acceptable limits for HIFU treatments. When the focal steering for sonication is within the safe steering range, the acoustic intensity at the focal region remains at an acceptable level. This characteristic is particularly advantageous in therapeutic scenarios that necessitate focal steering. Minimizing energy dispersion in a region such as the near-field grating lobes enables the concentration of emitted energy within the focal zone, without the requirement for substantial amplification of the output power of the HIFU system. Therefore, there are certain advantages to using this array design in clinical phased HIFU systems.

Skin burns and abdominal edema are common adverse events in clinical HIFU treatments, often associated with poor skin coupling and localized high acoustic intensity along the beam path (Mougenot et al., 2011). As the transducer gets closer to the human body, the surface area of the skin penetrated by the acoustic beam increases. Considering the relatively small changes in peak focal pressure during axial focal steering of the Fibonacci lattice array, we investigated a sonication strategy referred to as “near-field focusing”. This strategy involves steering the focus to the near field region of the transducer’s geometric center during sonication.

In this study, when the transducer is displaced from a distance of 95 mm to a position of 75 mm relative to the coupling pad, the surface area of the skin traversed by the HIFU beam is enlarged twofold. Consequently, the average acoustic intensity on the skin surface within this region is expected to diminish by about 50% compared to the previous condition. Adoption of this strategy can effectively mitigate the clinical treatment risks associated with skin burn caused by excessive acoustic intensity on the skin surface. It may also aid in reducing the incidence of abdominal edema.

Additionally, according to our simulations, both the Fibonacci lattice array and the Fermat's spiral array show an intriguing feature: the grating lobes arising due to focal steering have a distinct wreath-like pattern encircling the *Z*-axis, and their position remains relatively stable. For instance, in the specific array arrangement used in this study, this position was about 20–25 mm anterior to the geometric focal point. Therefore, compared to the case without focal steering, when the focus is axially steered to a position of −20 mm, the near-field region may become "cleaner". This is because the positions where grating lobes tend to occur are aligned mainly with the focal plane. This may help to reduce the temperature rise in the prefocal region.

To validate this conjecture, we conducted phantom sonication experiments using both rapid scanning ablation and rapid scanning combined with the near-field focusing strategy. MR thermometry revealed that using the near-field focusing strategy did not significantly reduce the ablation volume and effectively suppressed temperature elevation in the prefocal region.

During the clinical procedure of HIFU ablation therapy, it is essential to arrange focal points densely within tumors to ensure complete tumor coverage (Haar and Coussios, 2007). Consequently, the anterior region of the tumor is exposed to multiple heating events due to the overlapping of acoustic beams, giving rise to safety concerns such as the occurrence of abdominal edema. The implementation of a near-field focusing strategy can effectively reduce the treatment risks associated with ablation of large-volume tumors.

There were several limitations in this study. Firstly, we did not assess the performance of the fully populated phased arrays generated using the Fibonacci lattice. This was because we had not completed the fabrication of such transducers, preventing us from conducting experimental validation of their acoustic performance and ablative capabilities. Secondly, the three-layered medium model that we used was relatively simplistic, lacking the ability to fully capture the intricate impact of complex, multi-layered tissue structures in the human body during clinical treatment. Lastly, our ablation experiments on the phantom used a consistent ablation depth and a fixed sonication strategy. While theoretically, such a focusing strategy would be beneficial for ablation at different tissue depths, the practical efficacy of this focusing strategy warrants further comprehensive experimental assessment.

5 Conclusions

In this study, a novel element arrangement method was proposed for therapeutic phased array HIFU transducers that enables a more uniform and asymmetric distribution of piston elements on a spherical transducer surface. When applying the Voronoi tessellation to this element arrangement, the resulting fully populated array showed excellent uniformity of element areas. Simulation results indicated that using this element arrangement method can significantly increase the focal steering range and reduce the decline in peak focal pressure. Additionally, considering the acoustic field characteristics of the phased array, a "near-field focusing" strategy was introduced to reduce the average acoustic intensity on the skin surface during clinical treatment. Experimental results showed that this strategy effectively reduces the temperature elevation in the prefocal region, consequently mitigating safety risks during clinical treatment.

Acknowledgments

This work is supported by the National Key Research and Development Program of the Ministry of Science and Technology (Nos. 2022YFC2406900 and 2017YFC0108900), the National Natural Science Foundation of China (Nos. 81727806 and 11774231), the Shanghai Technical Leader (No. 20XD1432300), the Ningbo 2025 Key Research Program, the 2017 Key Project of Shanghai Science and Technology Commission (No. 17441906400), and the 2015 Key Project of Shanghai Science and Technology Commission (No. 15441900700).

Author contributions

Xiongfei QU designed the research, processed the corresponding data, and wrote the first draft of the manuscript. Nan WU and Yazhu CHEN helped to organize the manuscript. Guofeng SHEN and Xiongfei QU revised and edited the final version.

Conflict of interest

Xiongfei QU, Nan WU, Yazhu CHEN, and Guofeng SHEN declare that they have no conflict of interest.

References

Agrawal M, Garg K, Samala R, et al., 2021. Outcome and complications of MR guided focused ultrasound for essential tremor: a systematic review and meta-analysis. *Frontiers in Neurology*, 12:654711. https://doi.org/10.3389/fneur.2021.654711

Bachu VS, Kedda J, Suk I, et al., 2021. High-intensity focused ultrasound: a review of mechanisms and clinical

applications. *Annals of Biomedical Engineering*, 49(9): 1975-1991. https://doi.org/10.1007/s10439-021-02833-9

Brauchart JS, Grabner PJ, 2015. Distributing many points on spheres: minimal energy and designs. *Journal of Complexity*, 31(3):293-326. https://doi.org/10.1016/j.jco.2015.02.003

Chaussy CG, Thüroff S, 2017. High-intensity focused ultrasound for the treatment of prostate cancer: a review. *Journal of Endourology*, 31(S1):S-30-S-37. https://doi.org/10.1089/end.2016.0548

Chukkapalli G, Karpik SR, Ethier CR, 1999. A scheme for generating unstructured grids on spheres with application to parallel computation. *Journal of Computational Physics*, 149(1):114-127. https://doi.org/10.1006/jcph.1998.6146

Damianou C, Hynynen K, 1993. Focal spacing and near-field heating during pulsed high temperature ultrasound therapy. *Ultrasound in Medicine & Biology*, 19(9):777-787. https://doi.org/10.1016/0301-5629(93)90094-5

Daum DR, Hynynen K, 1998. Thermal dose optimization via temporal switching in ultrasound surgery. *IEEE Transactions on Ultrasonics, Ferroelectrics and Frequency Control*, 45(1):208-215. https://doi.org/10.1109/58.646926

Diederich CJ, Hynynen K, 1999. Ultrasound technology for hyperthermia. *Ultrasound in Medicine & Biology*, 25(6): 871-887. https://doi.org/10.1016/s0301-5629(99)00048-4

Ellens N, Pulkkinen A, Song J, et al., 2011. The utility of sparse 2D fully electronically steerable focused ultrasound phased arrays for thermal surgery: a simulation study. *Physics in Medicine and Biology*, 56(15):4913-4932. https://doi.org/10.1088/0031-9155/56/15/017

Garcia-Gutierrez CM, Becerra-Herrejon H, Garcia-Becerra CA, et al., 2022. High intensity focused ultrasound (HIFU) in prostate diseases (benign prostatic hyperplasia (BPH) and prostate cancer). *In*: Arnouk H (Ed.), Advances in Soft Tissue Tumors. IntechOpen, London, UK. https://doi.org/10.5772/intechopen.102663

Gavrilov LR, Hand JW, 2000. A theoretical assessment of the relative performance of spherical phased arrays for ultrasound surgery. *IEEE Transactions on Ultrasonics, Ferroelectrics and Frequency Control*, 47(1):125-139. https://doi.org/10.1109/58.818755

González Á, 2010. Measurement of areas on a sphere using Fibonacci and latitude–longitude lattices. *Mathematical Geosciences*, 42(1):49-64. https://doi.org/10.1007/s11004-009-9257-x

Goss SA, Frizzell LA, Kouzmanoff JT, et al., 1996. Sparse random ultrasound phased array for focal surgery. *IEEE Transactions on Ultrasonics, Ferroelectrics and Frequency Control*, 43(6):1111-1121. https://doi.org/10.1109/58.542054

Haar GT, Coussios C, 2007. High intensity focused ultrasound: physical principles and devices. *International Journal of Hyperthermia*, 23(2):89-104. https://doi.org/10.1080/02656730601186138

Hüttig C, Stemmer K, 2008. The spiral grid: a new approach to discretize the sphere and its application to mantle convection. *Geochemistry, Geophysics, Geosystems*, 9(2):Q02018. https://doi.org/10.1029/2007GC001581

Ji YS, Zhu JQ, Zhu LL, et al., 2020. High-intensity focused ultrasound ablation for unresectable primary and metastatic liver cancer: real-world research in a Chinese tertiary center with 275 cases. *Frontiers in Oncology*, 10: 519164. https://doi.org/10.3389/fonc.2020.519164

Kennedy JE, Ter Haar GR, Cranston D, 2003. High intensity focused ultrasound: surgery of the future? *The British Journal of Radiology*, 76(909):590-599. https://doi.org/10.1259/bjr/17150274

Kim YS, Keserci B, Partanen A, et al., 2012. Volumetric MR-HIFU ablation of uterine fibroids: role of treatment cell size in the improvement of energy efficiency. *European Journal of Radiology*, 81(11):3652-3659. https://doi.org/10.1016/j.ejrad.2011.09.005

Klíma K, Pick M, Pros Z, 1981. On the problem of equal area block on a sphere. *Studia Geophysica et Geodaetica*, 25(1): 24-35. https://doi.org/10.1007/BF01613559

Kociuba J, Łoziński T, Zgliczyńska M, et al., 2023. Adverse events and complications after magnetic resonance-guided focused ultrasound (MRgFUS) therapy in uterine fibroids–a systematic review and future perspectives. *International Journal of Hyperthermia*, 40(1):2174274. https://doi.org/10.1080/02656736.2023.2174274

Köhler MO, Mougenot C, Quesson B, et al., 2009. Volumetric HIFU ablation under 3D guidance of rapid MRI thermometry. *Medical Physics*, 36(8):3521-3535. https://doi.org/10.1118/1.3152112

Lam MK, Huisman M, Nijenhuis RJ, et al., 2015. Quality of MR thermometry during palliative MR-guided high-intensity focused ultrasound (MR-HIFU) treatment of bone metastases. *Journal of Therapeutic Ultrasound*, 3(1):5. https://doi.org/10.1186/s40349-015-0026-7

Marinova M, Ghaei S, Recker F, et al., 2021. Efficacy of ultrasound-guided high-intensity focused ultrasound (USgHIFU) for uterine fibroids: an observational single-center study. *International Journal of Hyperthermia*, 38(2): 30-38. https://doi.org/10.1080/02656736.2021.1939444

Mougenot C, Köhler MO, Enholm J, et al., 2011. Quantification of near-field heating during volumetric MR-HIFU ablation. *Medical Physics*, 38(1):272-282. https://doi.org/10.1118/1.3518083

Muller ME, 1959. A note on a method for generating points uniformly on *n*-dimensional spheres. *Communications of the ACM*, 2(4):19-20. https://doi.org/10.1145/377939.377946

Quadri SA, Waqas M, Khan I, et al., 2018. High-intensity focused ultrasound: past, present, and future in neurosurgery. *Neurosurgical Focus*, 44(2):E16. https://doi.org/10.3171/2017.11.FOCUS17610

Rakhmanov EA, Saff EB, Zhou YM, 1994. Minimal discrete energy on the sphere. *Mathematical Research Letters*, 1(6):

647-662.
https://doi.org/10.4310/MRL.1994.v1.n6.a3

Ramaekers P, de Greef M, Berriet R, et al., 2017a. Evaluation of a novel therapeutic focused ultrasound transducer based on Fermat's spiral. *Physics in Medicine and Biology*, 62(12): 5021-5045.
https://doi.org/10.1088/1361-6560/aa716c

Ramaekers P, Ries M, Moonen CTW, et al., 2017b. Improved intercostal HIFU ablation using a phased array transducer based on Fermat's spiral and Voronoi tessellation: a numerical evaluation. *Medical Physics*, 44(3):1071-1088.
https://doi.org/10.1002/mp.12082

Rosnitskiy PB, Vysokanov BA, Gavrilov LR, et al., 2018. Method for designing multielement fully populated random phased arrays for ultrasound surgery applications. *IEEE Transactions on Ultrasonics, Ferroelectrics, and Frequency Control*, 65(4):630-637.
https://doi.org/10.1109/TUFFC.2018.2800160

Rosnitskiy PB, Sapozhnikov OA, Gavrilov LR, et al., 2020. Designing fully populated phased arrays for noninvasive ultrasound surgery with controlled degree of irregularity in the arrangement of elements. *Acoustical Physics*, 66(4): 352-361.
https://doi.org/10.1134/S1063771020040090

Swinbank R, James Purser R, 2006. Fibonacci grids: a novel approach to global modelling. *Quarterly Journal of the Royal Meteorological Society*, 132(619):1769-1793.
https://doi.org/10.1256/qj.05.227

Ter Haar GR, 2001. High intensity focused ultrasound for the treatment of tumors. *Echocardiography*, 18(4):317-322.
https://doi.org/10.1046/j.1540-8175.2001.00317.x

Uchida T, Nakano M, Hongo S, et al., 2012. High-intensity focused ultrasound therapy for prostate cancer. *International Journal of Urology*, 19(3):187-201.
https://doi.org/10.1111/j.1442-2042.2011.02936.x

Vyas U, Christensen D, 2012. Ultrasound beam simulations in inhomogeneous tissue geometries using the hybrid angular spectrum method. *IEEE Transactions on Ultrasonics, Ferroelectrics and Frequency Control*, 59(6):1093-1100.
https://doi.org/10.1109/TUFFC.2012.2300

Zhao H, Yang GW, Wang DY, et al., 2010. Concurrent gemcitabine and high-intensity focused ultrasound therapy in patients with locally advanced pancreatic cancer. *Anti-Cancer Drugs*, 21(4):447-452.
https://doi.org/10.1097/CAD.0b013e32833641a7

Zhou YF, 2011. High intensity focused ultrasound in clinical tumor ablation. *World Journal of Clinical Oncology*, 2(1): 8-27.
https://doi.org/10.5306/wjco.v2.i1.8

Ziglioli F, Baciarello M, Maspero G, et al., 2020. Oncologic outcome, side effects and comorbidity of high-intensity focused ultrasound (HIFU) for localized prostate cancer. A review. *Annals of Medicine and Surgery*, 56:110-115.
https://doi.org/10.1016/j.amsu.2020.05.029